

## Investigation on the Transcritical Behaviour of Methane and Numerical Rebuilding Activities in the Framework of ASI/JAXA Cooperation Project

D. Ricci<sup>1</sup>, P. Natale<sup>1</sup>, F. Battista<sup>1</sup>, E. d'Aversa<sup>2</sup>, R. Pellegrini<sup>2</sup>, H. Asakawa<sup>3</sup>, H. Negishi<sup>3</sup>

<sup>1</sup>CIRA (Italian Aerospace Research Centre) - Via Maiorise, 81043 Capua (CE), Italy

<sup>2</sup>ASI (Italian Space Agency) - Via del Politecnico, 00133 Rome, Italy

<sup>3</sup>JAXA (Japan Aerospace Exploration Agency) - 2-1-1 Sengen, Tsukuba-shi, Ibaraki-ken, 305-8508 Japan

**KEYWORDS:** Liquid Rocket Engine, Methane, Transcritical Behaviour, Numerical Simulation.

### 1. ABSTRACT

The Italian Space Agency (ASI) and Japan Aerospace Exploration Agency (JAXA) have recently promoted a program in order to co-operate in the research and development fields of liquid oxygen-liquid methane based space propulsion systems. In particular, the two National Agencies agreed to share the efforts into design, manufacture and test a 100 kN regeneratively-cooled demonstrator.

Different development lines were started, led by ASI/AVIO for the Italian side and JAXA/IHI for the Japanese one. The Italian Aerospace Research Center (CIRA) received the commitment to performing the design analyses concerning the injector head, its propellant distribution system, and the integration with the thrust chamber and the cooling jacket, realized by the Japanese partners. However, in the first phase of the program, a basic research activity on the investigation about the transcritical behaviour of methane has been planned and carried out by CIRA and JAXA.

A specific breadboard, named MTP-BB (Methane Thermal Properties Breadboard), has been designed and tested by CIRA for these purposes; the experimental results have been analysed and rebuilt by means of numerical simulations.

In this paper, after a brief summary of the experimental test campaign by CIRA the numerical rebuilding activity performed by CIRA and JAXA is presented.

### 2. BACKGROUND

The industrial and scientific communities are addressing major research efforts to identify and assess critical technologies for new advanced propulsive concepts: combustion at high pressure, as well as the replacement of hydrogen with a hydrocarbon, lower environmental impact, reduction of the costs, related to ground operations, increase in terms of flexibility, etc. [1]. LOX/Methane propulsion seems to be in line with these goals [2, 3], thus, some important projects have been launched to investigate critical aspects and consolidate the technology, based on LOX/LCH<sub>4</sub> [4-6]. In this view, ASI and JAXA have recently signed a co-operation agreement in order to take advantage of the technological background and expertise, developed in previous respective National programs. Important Italian and Japanese aerospace industries, AVIO and

IHI, have been involved. Both the industries have an important and recognized know-how in space propulsion, developed in previous R&D projects (MIRA and HYPROB on the Italian side and several firing tests on LNG-based demonstration engines on the Japanese side).

The final goal of ASI/JAXA Cooperation Program is the integration and the improvement of respective competences and capabilities in order to allow each actor to design and realize autonomously a methane-based LRE (Liquid Rocket Engine).

The Program is organized in three lines, concerning the following issues:

- 1) thermal and fluid-dynamic characterization of methane as refrigerant in supercritical conditions;
- 2) characterization of methane turbo-pump bearings;
- 3) development of a joint ASI-JAXA regenerative cooled thrust chamber (100-kN-thrust class).

The first task has the objective to investigate the thermal behaviour of methane in LRE operative conditions in order to improve know-how, design tools and numerical codes. Only a wide experimental database may bring to the validation of procedures and this will be achieved by conducting tests in parallel on relevant specimen, by exchanging information and comparing results.

The second task includes all the activities regarding the development of new competences on the operability of turbo-pump roller bearings, cooled by liquid methane. In this framework, some area of interest have been identified, such as methane cooling capabilities, basic materials behaviour, verification of influence of the most significant test parameters (pressure, temperature, rpm, etc.). In addition, this task foresees a tighten co-operation between the partners, aimed at performing tests in parallel and consequent cross-check activity.

The objective of the third task is the design, realization and test of a joint ASI-JAXA regeneratively cooled thrust chamber, characterized by a thrust of 100 kN on ground. The following area of interest will be investigated: verification of operability in different domains (O/F, chamber pressure); verification of methane cooling capabilities; verification of performance ( $c^*$ ) and effects of O/F shifts; verification of stability.

CIRA has been directly involved in the first line and the second line, performing the design analyses concerning the injector head, its propellant distribution system, and the integration with the thrust chamber and the cooling jacket, realized by the Japanese partners.

### 3. MOTIVATIONS

Rocket engine thrust chambers must withstand huge thermal and mechanical loads. This is achieved by means of efficient cooling systems, whose development is performed by deeply investigating the fluid behavior inside the cooling channels and the heat transfer processes, involved in thrust chambers and coupled with the cooling jacket [7]. This is particularly important in the case of regeneratively cooled modern liquid rocket engines, which may use propellants (H<sub>2</sub>, CH<sub>4</sub>), eventually behaving as supercritical fluids. [8].

The reliable operation of rocket combustion chamber at such high thermal and mechanical loads is achieved with highly efficient cooling. For optimal cooling design with minimal hydrodynamic losses the precise knowledge of heat transfer processes in rocket engines and particularly in cooling channel is important. Moreover, the supercritical state of the propellant represent a strong complication in the design loop.

However, the supercritical condition may bring to some complications in the design phases, in particular in the case of methane [9]. In fact, the evaluation of heat transfer coefficients and the estimation of pressure losses are based on approaches, affected by a reduced predictivity, especially in the case of the complex geometries, unsymmetrical heat flux boundary conditions, due to poor experimental data sets [11]. Thus, the collection of experimental data, in the operative conditions of rocket engine cooling jackets, is demanded also to validate both simplified design tools and numerical methods or codes, adopted for the detailed analysis phases [12].

In this view, the present MTP Breadboard (Methane Thermal Properties) has been designed to provide information about methane behavior in supercritical conditions and investigate important phenomenon, like the temperature stratification in the cooling channels and heat transfer deterioration [13]. As in a typical channel, belonging to a LRE cooling jacket, methane enters the MTP at pressure and temperature values higher than the critical one ( $P_{cr} = 4.59$  MPa and  $T_{cr} = 190.56$  K), respectively. The fluid is gradually heated and, along the axial direction pressure, tends to decrease and temperature rises until reaching the critical value and beyond. In fact, in the MTP the fluid works at a pressure values, ranging from 6.0 to 15.0 MPa, and is injected at an inlet temperature value of about 130-140 K while the outlet one is about 240-260 K. As a result, the fluid goes out as a supercritical vapour since a “pseudo-change” from a liquid-like condition to a vapour-like is achieved (see Figure 1).

It is important to underline that around the critical point, the fluid experiences a gradual but very significant variation of thermo-physical properties (density, viscosity, specific heat, thermal conductivity, etc.), as depicted by Figure 2, where thermal conductivity is plotted as a function of temperature and pressure.

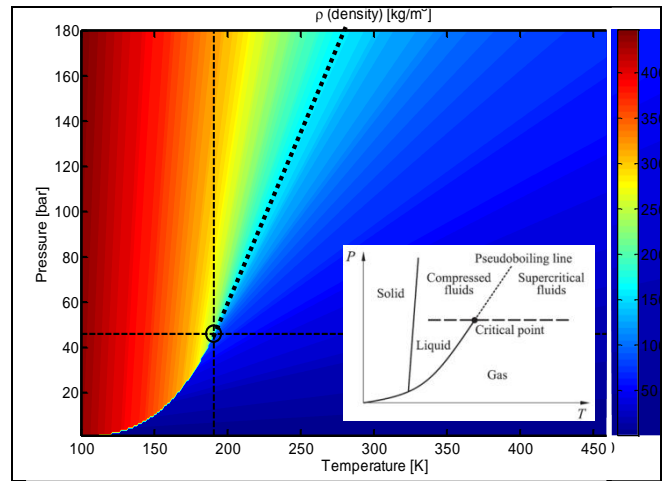


Figure 1 - Methane thermo-physical properties, as a function of temperature and pressure: density, derived by NIST [14]

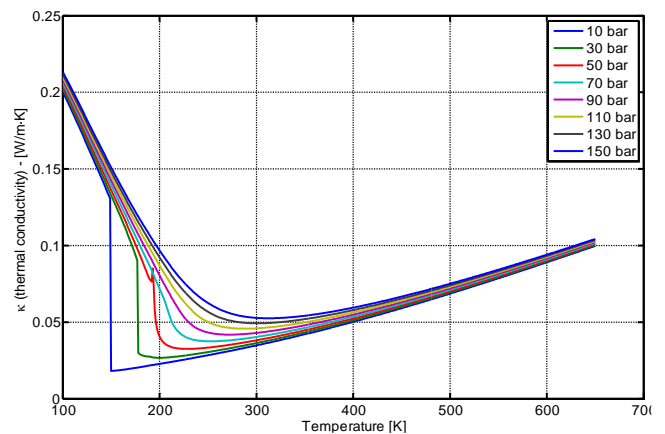


Figure 2 - Methane thermo-physical properties, as a function of temperature and pressure: thermal conductivity, derived from NIST [14]

The specific heat profiles as a function of temperature and pressure are very important to be observed in order to understand the thermal performances of supercritical fluids. In fact, around the so-called pseudo-critical point, specific heat reaches a maximum at this particular pressure. The corresponding temperature is called pseudo-critical temperature ( $T_{pc} > T_{cr}$ ) and it increases as pressure increases while the specific heat peak value reduces, up to vanish at very high values of pressure, as depicted by Figure 3. Near this point, in literature authors agree that a significant deterioration of the fluid thermal performances may be observed: the fluid is characterized by low thermal conductivity near the hot walls (where behaves like a vapour) while the core exhibit very high values of specific heat [15-17]. The risk of deterioration is higher in correspondence with operating pressures, near to the critical one, and for low roughness values of the channel walls [17]. It is important to investigate this behaviour since the typical correlations result to be not suitable to describe the heat transfer exchange.

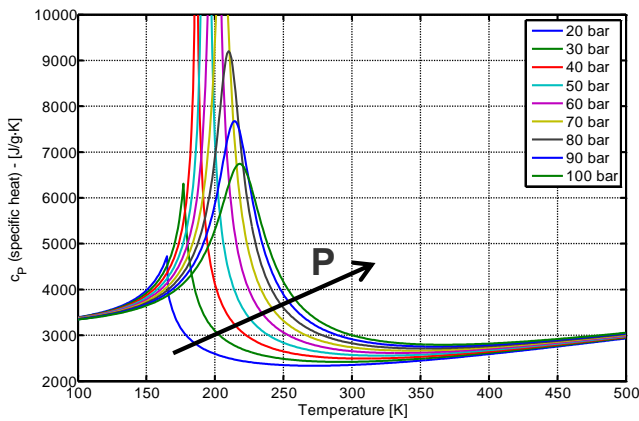


Figure 3 - Methane thermo-physical properties, as a function of temperature and pressure: specific heat, derived from NIST [14]

#### 4. TEST ARTICLE DESCRIPTION

MTP Breadboard is made up of a copper alloy block where a narrow rectangular channel is realized on the top. In the bottom part, ten cylindrical housings are located to host the electrical cartridges, which generate the thermal loads (similar to ones experienced in a LRE cooling jacket) by means of the Joule effect (20 kW of maximum power). The test article, depicted in Figure 4, has a rectangular basement and it has been shaped in order to 'drive' the heat towards the top, where the channel is located.

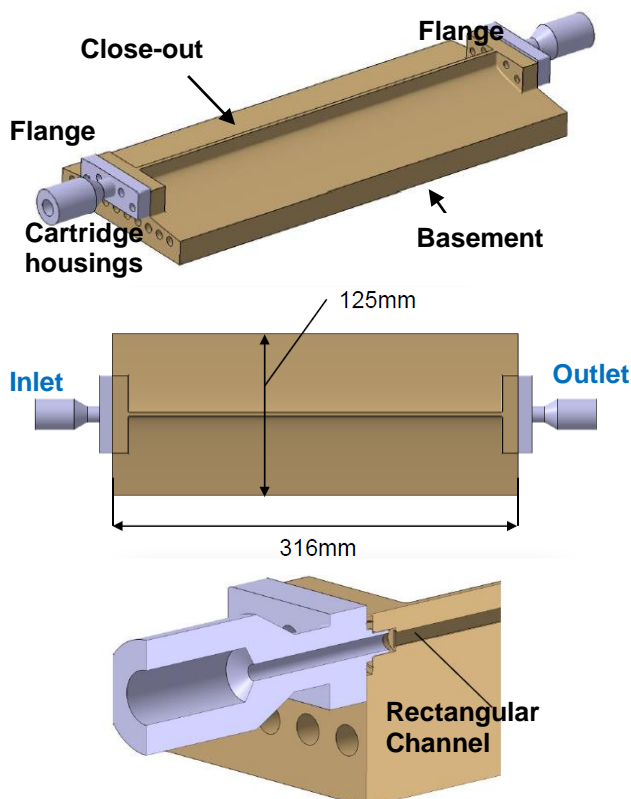


Figure 4 - Sketch of the MTP test article with geometric information and detail on the inlet/outlet fluidic interface

The total length (including the fluidic/mechanical flanges) and width are equal to 316 mm and 125 mm, respectively. The rectangular channel has an aspect ratio,  $a/b$ , equal to 3 ( $a = 3$  mm and  $b = 1$  mm) and an

effective length of 292 mm. At the inlet and outlet sections, two mechanical interfaces, threaded and sealed, are located in order to achieve an easy connection to the test facility supply: they have a length of 10 mm each and pressure/temperature sensors are allocated in the middle.

#### 5. TEST ARRANGEMENT DESCRIPTION

Tests were successfully conducted at the Maurice J. Zucrow Laboratories, Purdue University. The facility supplied the electrical power (a three phase electrical power source, manually activated) and the fluid (gaseous methane was liquefied by a condenser, in-house designed and realized, adopting LN<sub>2</sub>). The fluid was heated in order to obtain the phase "pseudo-change" through the critical conditions and beyond until reaching the pseudo-critical conditions for each test. The connection to the facility feed system was ensured by inlet/outlet flanges, presented in Figure 10.

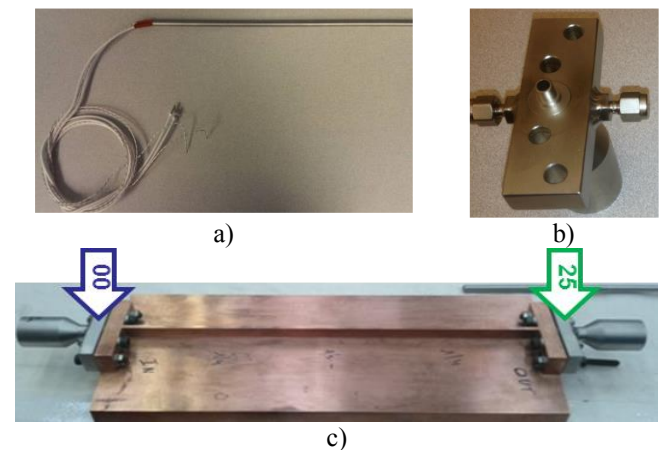


Figure 5 - MTP test arrangement: a) electrical cartridge; b) IFs detail with the housing of sensors; c) Position of the temperature and pressure in/out sensors

The breadboard was equipped with K-type with the extremities oriented towards the bottom surface of the channel. Moreover, they were placed at different depth (4, 10 and 16 mm from the bottom channel walls), being divided into groups of 3 since: the distance between two consecutive stations is 60 mm.

The mass flow was measured by means of a cavitating Venturi and regulated by a control valve, located downstream the MTP. During the tests, the article was thermally insulated to avoid losses of heat power throughout external walls by a ceramic blanket, as pointed out by Figure 6. Briefly, the operative phase consisted into purging the breadboard channel by means LN<sub>2</sub> and consequently switching the heat source on. Then, after reaching quasi-steady state conditions the LCH<sub>4</sub> flow command was manually given in order to perform each experimental test.

Before starting the test campaign, leak and proof tests were accomplished and for each test condition, two tests were conducted for repeatability purposes. The test matrix included the following test conditions:

- mass flow rate: 15, 20, 25 g/s
- exit pressure: 8.0, 10.0, 12.0, 15.0 MPa;
- electrical power: 0 (cold flow), 12 kW;

- inlet fluid temperature: 120, 140 K.

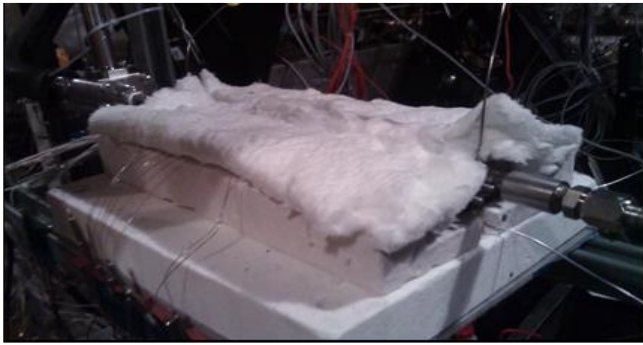


Figure 6 - MTP on the bench, during a test

## 6. NUMERICAL REBUILDING ACTIVITY

A numerical rebuilding activity was planned to in-depth the comprehension of the test results. The computational domain, included the MTP model, cut 6 mm below the bottom channel surface, and also half inlet and outlet interfaces were considered in order to take into account the position of inlet/outlet pressure and temperature sensors.

Simulations were accomplished by means of ANSYS Fluent v14© [18] on a 3-D model and two hot tests were performed after completing a preliminary activity on two cold flow tests.

The governing equations of continuity, momentum and energy in the 3-D form were solved under the hypothesis of steady state, NIST real gas model (REFPROP v7.0 database) and turbulent flow. Also the conduction effects were taken into account and the channel surfaces were considered rough. Both the solid and fluid parts were included in the computational domain and a particular attention was paid in the meshing phase in order to provide continuity in terms of nodes' number. Moreover, different turbulence models were adopted ( $k-\omega$  std,  $k-\omega$  sst,  $k-\epsilon$  std) [18]. A pressure-based method was adopted while a second-order upwind scheme and the SIMPLEC coupling one were chosen for energy and momentum equations and to couple pressure and velocity, respectively. The convergence criteria of  $10^{-6}$  and  $10^{-10}$  for the residuals of the velocity components and energy were assumed, respectively.

Simulations were initialized at the inlet section conditions in terms of fluid temperature and pressure, according to the chosen test. The NIST real gas model was activated in the form of single-species flow since it is able to handle both the liquid phase and the vapour one.

With reference to, the considered solid material was a copper alloy (orange). Half channel was simulated in order to reduce the computational effort, applying a symmetry condition exploiting the geometrical and thermo-fluid dynamic symmetry; the upper wall and left external one were considered adiabatic while the bottom surface of the model was heated by a constant heat flux. The outlet part was enlarged for convergence purposes (the length is six times the  $D_h$  of the actual outlet tube).

The adopted mesh distribution is a structured grid of about 2.7 million nodes; some information on the nodes' distribution in the axial direction and in the channel section is given in Figure 14.

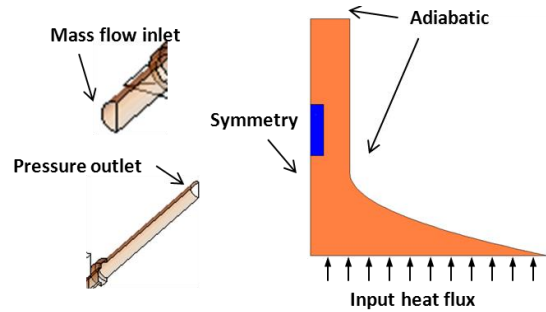


Figure 7 - Sketch of the model and applied boundary conditions

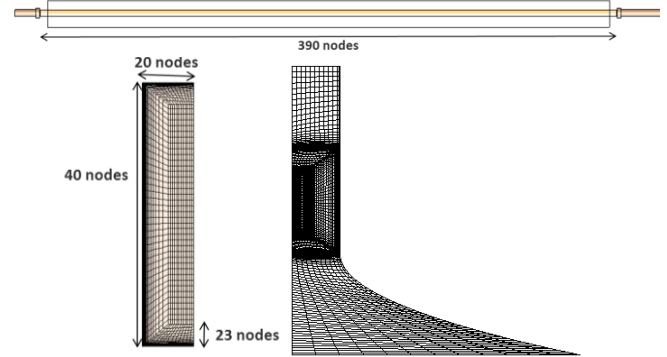


Figure 8 - Mesh distribution information on axial direction and channel section

The final wall refinement is equal to  $0.4 \mu\text{m}$  and a particular attention has been paid for meshing expansion/contraction sections (see Figure 9).

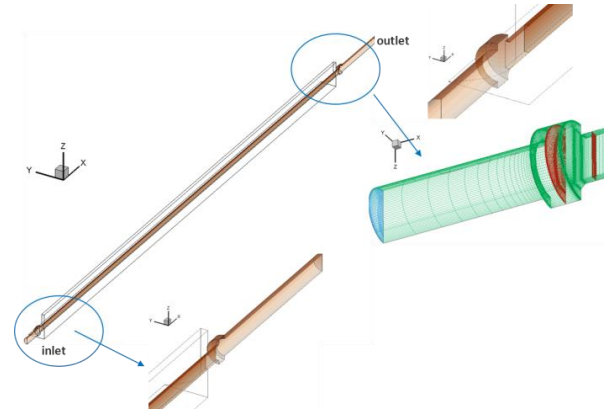


Figure 9 - Mesh distribution details on the inlet/outlet sections

## 7. RESULTS AND DISCUSSION

Results are presented for some of the test cases, experimentally investigated and rebuilt by means of CFD analyses. An extract of results obtained for the experimental test cases, considered here, is reported in Table 1: two cold flow tests and two hot flow tests were numerically rebuilt by means of a specific simulation campaign (the CIRA test matrix is reported by Table 2).

Table 1 - Considered experimental test cases

TEST	Steady state time [s]	$\dot{m}$ [g/s]	$T_{in}$ [K]	$T_{out}$ [K]	$P_{in}$ [bar]	$P_{out}$ [bar]
42	135	15.72	133.0	135.0	87.66	84.71
43	90	25.92	126.0	130.0	88.11	80.18
24	225	20.87	137.1	244.6	111.72	103.1
26	255	20.57	140.8	262.8	129.1	120.6

Cold flow tests, Hot flow tests

Table 2 – CIRA test matrix of numerical rebuilding campaign

RUN	TEST	mesh	Turb. model	Power [kW]
0	-----	Coarse	k- $\omega$ sst	0
1	42	Coarse	k- $\omega$ sst	0
2	42	Fine	k- $\omega$ sst	0
3	42	Fine	k- $\omega$ std	0
4	42	Coarse	k- $\epsilon$ swf	0
5	43	Fine	k- $\omega$ sst	0
6	24	Fine	k- $\omega$ sst	10.7
7	26	fine	k- $\omega$ sst	11.0

Cold flow tests, Hot flow tests

In particular, the cold flow tests (test 42 and 43) were performed in order to evaluate the roughness of the channel since the manufacturing supplier provided measurement results only for a mock-up version of the MTP channel. Cold flows were also useful to set the roughness model in Fluent© code and perform some tests on the grids and turbulence models (k- $\omega$  std, k- $\omega$  sst and k- $\epsilon$  swf). A brief summary of the CFD results is shown by Table 3: it anticipates that both cold tests and hot ones were rebuilt with low discrepancies with respect to the experimental results. Simulations were accomplished considering steady-state formulation and, thus, the comparisons were performed at a test time, representative of this state.

Table 3 - Summary of CFD results about the numerical rebuilding campaign

RUN	T <sub>in</sub> [K]	T <sub>out</sub> [K]	$\Delta T\%$	P <sub>in</sub> [bar]	P <sub>out</sub> [bar]	$\Delta P\%$
0	133	133	-----	86.12	84.71	-----
1	133	133	-----	87.57	84.71	-3.1%
2	133	133	-----	87.63	84.71	-0.3%
3	133	133	-----	87.65	84.71	-1.0%
4	133	133	-----	87.64	84.71	-0.7%
5	126	126	-----	87.88	80.18	-2.9%
6	137	245.3	0.7%	111.72	111.72	-5.3%
7	141	261.0	-1.7%	129.10	129.1	2.0%

Cold flow tests

As aforementioned, CIRA conducted a preliminary phase on cold flow tests to estimate the channel average roughness and the set-up of the roughness numerical model. The starting point was the evaluation of the concentrated and distributed losses. This was accomplished by means of engineering formula [19, 20], considering the sketch of Figure 10, and a comparison with engineering tools (Ecosimpro©) was carried out. Thus, the sand-grain roughness value of the channel was estimated by means of the Moody’s chart, knowing the Reynolds number inside the channel ( $Re = \rho V D h / \mu \sim 92000$  and  $\sim 139000$  for test 42 and 43, respectively), the geometric features and the derived distributed pressure drops.

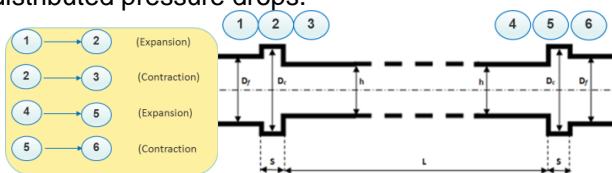
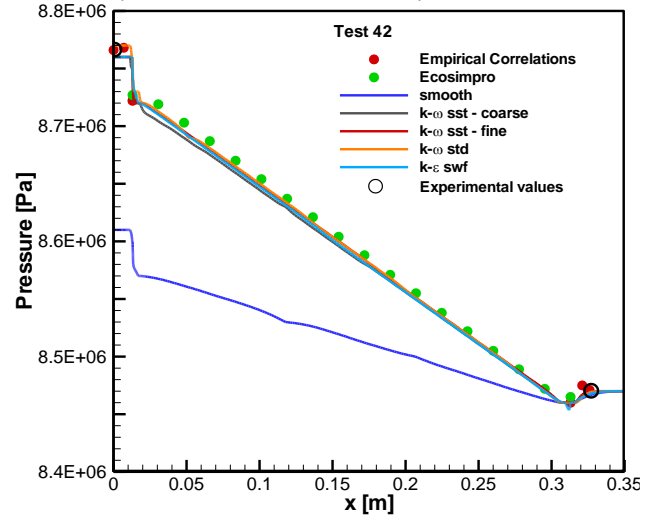
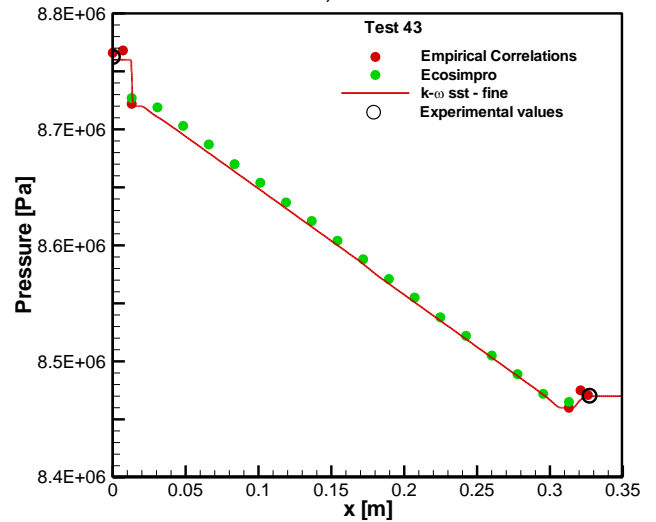


Figure 10 - Sketch of the MTP channel for the evaluation of pressure drops

The evaluated average value was about  $14.5 \mu m$  and this value was adopted for all the numerical campaign. A grid sensitivity test was performed by considering two mesh distributions, adopting the k- $\omega$  sst turbulence model: a coarse one with 1.4 million nodes and a fine one, characterized by about 2.7 million nodes and a wall refinement of  $0.4 \mu m$ . The finer mesh was chosen for the hot tests since a reduction of error with respect to experimental results in terms of pressure drops was observed (from 3.1% to about 0.3%) for test 42.



a)



b)

Figure 11 - Preliminary phase - estimation of sand-grain roughness through cold flow tests and model sensitivity analysis: a) test 42; b) test 43

A comparison with other turbulence models was performed and showed little discrepancies, as depicted by Figure 11; thus, the k- $\omega$  sst was adopted for the simulation of test 43 and for the hot test ones, described in the next part of the section.

Hot flow tests

Two hot flow tests are here presented (test 24 and test 26). Figure 12 depicts the axial profiles in terms of pressure drops. Very low discrepancies are evaluated if a comparison with the experimental results (5.0% at maximum) is performed.

With respect to the aforementioned cold flow test results, pressure does not gradually decrease along the channel but decreases very significantly in the last part

of the channel. This is due to the phase “pseudo-change”, occurring in the channel: methane enters the channel as a compressed fluid and, after heated, its state changes from liquid-like state to gas-like. Thus, density decreases along the axial direction and as a result, velocity and pressure drops increase and this is more significant after reaching the critical conditions.

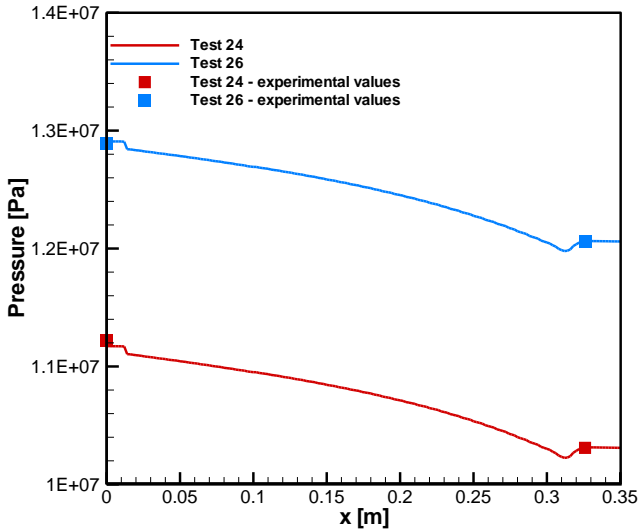


Figure 12 - Rebuilding of hot tests (24 and 26): pressure drops axial profiles

The critical temperature is achieved  $x = 0.13$  m and  $0.12$  m on average for test 24 and 26, respectively, as depicted by fluid bulk temperature profiles of Figure 13 while the pseudo-critical temperature is detected at about  $x = 0.23$  m. From this axial coordinate, the fluid can be considered as a supercritical vapour. Figure 13 indicates also very small differences of the numerical results if compared with the experimental ones in terms of the temperature values, evaluated at a depth of 4 mm from the channel bottom surface, and fluid inlet/outlet temperature (1.7% at maximum at the outlet section). Moreover, an important result is that the channel bottom surface temperature increases almost linearly in the axial direction for both tests. No abrupt deteriorations of thermal performances are detected since the operative pressure of both test 24 and 26 is quite far from the critical one (almost 4.6 MPa) and the channel roughness is relatively high. This influences also the wall temperature values, which are similar for the two tests, even in test case 26, characterized by a higher absorbed total power (11.0 against 10.7 kW). Consequently, also the thermal performances are quite similar, as depicted by the convective heat transfer coefficient axial profiles of Figure 14.

Test 24 exhibits convective heat transfer coefficient slightly higher than test 26 and the reason is linked to the “acceleration” of the fluid, due to the heating, which is more significant at lower pressure (the density decreasing becomes more evident, approaching the critical conditions).

After the entrance region, local heat transfer coefficient profiles tend to decrease, as expected, and the slope changes, approaching the critical point. Then, profiles seem to tend to an asymptotic value but after passing the x-coordinate, corresponding to the pseudo-critical point, local convective heat transfer values begin to increase towards the channel exit. The average

convective heat transfer coefficient profiles monotonically decrease towards the outlet section.

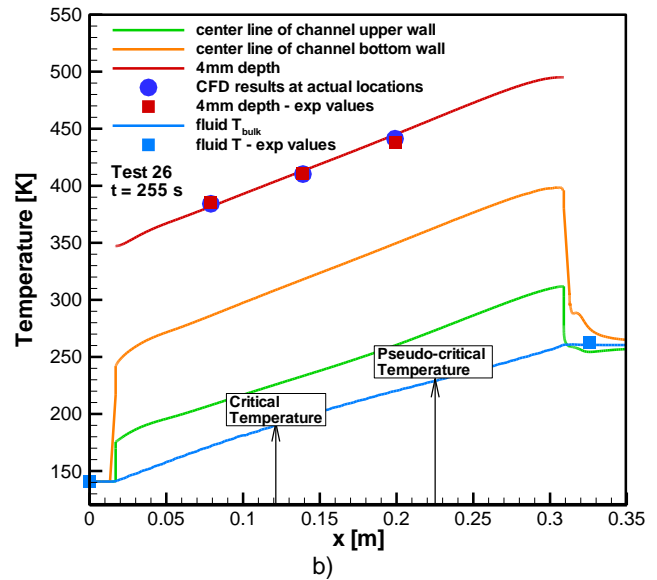
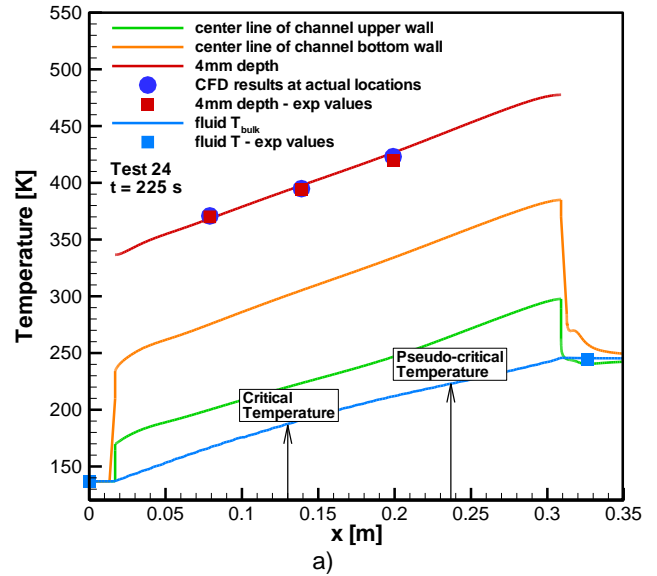


Figure 13 - Rebuilding of hot tests – Fluid temperature and bottom wall temperature profiles: a) test 24; b) test 26

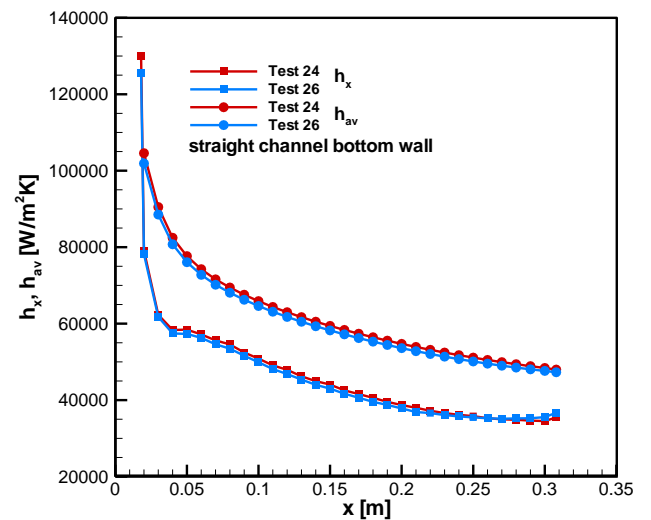


Figure 14 - Straight channel bottom wall: Local and average convective heat transfer coefficients

Figure 15 reports the axial profiles of density and specific heat. Density (as well as viscosity and thermal

conductivity, see next fields) decreases monotonically of about one order of magnitude if the inlet section is compared with outlet. In particular, this behaviour becomes very significant from  $x = 0.12$  m, such as in near-critical conditions. As aforementioned, the highest values of specific heat are detected at about  $x = 0.22$ - $0.24$  m.

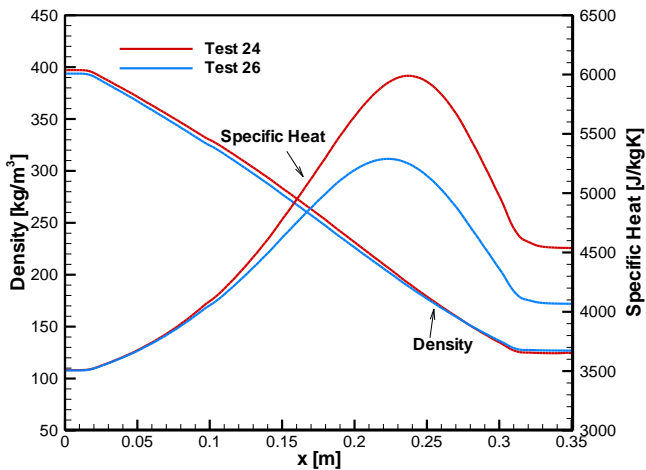


Figure 15 - Axial profile of density and specific heat

Figure 16 shows the temperature fields of the MTP walls, including some slices. The maximum temperature values are attained in the bottom part of the test article, near the external walls. Moving towards the top, the solid begins to feel the presence of the channel, which tends to uniform the temperature gradients near the channel bottom surface. On the top external wall, the breadboard exhibits very low temperature values as well as the lateral and the upper walls of the channel, which result slightly stressed.

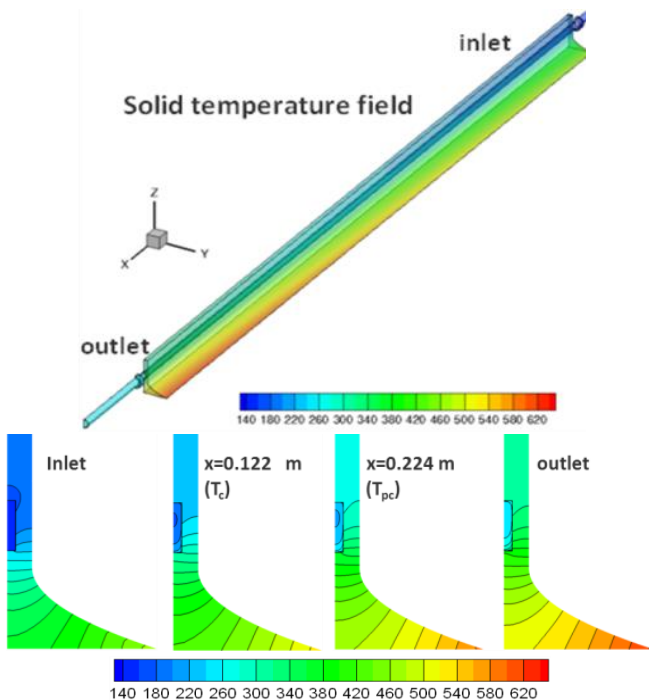


Figure 16 - Temperature distribution of the MTP walls, including some slices [K]

The description of methane in transcritical conditions may be accomplished through the fields of temperature, specific heat, density and thermal conductivity, reported

by Figure 17 for test 26. The fluid results to be hot in the lower part of the channel and near the right wall (on the right part) while, moving towards the top, temperature is significantly lower (i.e. fluid thermal stratification [22]). At about  $x = 0.122$  m the fluid reaches the critical temperature on average. From this section, the thermal stratification is evident: a part of the fluid, near the bottom wall, behaves like a “gas” while in the upper part keeps behaving like a “liquid”. After  $x = 0.224$  methane completely behaves like a supercritical vapour (the fluid bulk temperature is higher than the pseudo-critical one). This is also confirmed by the aforementioned density profile and specific heat distribution.

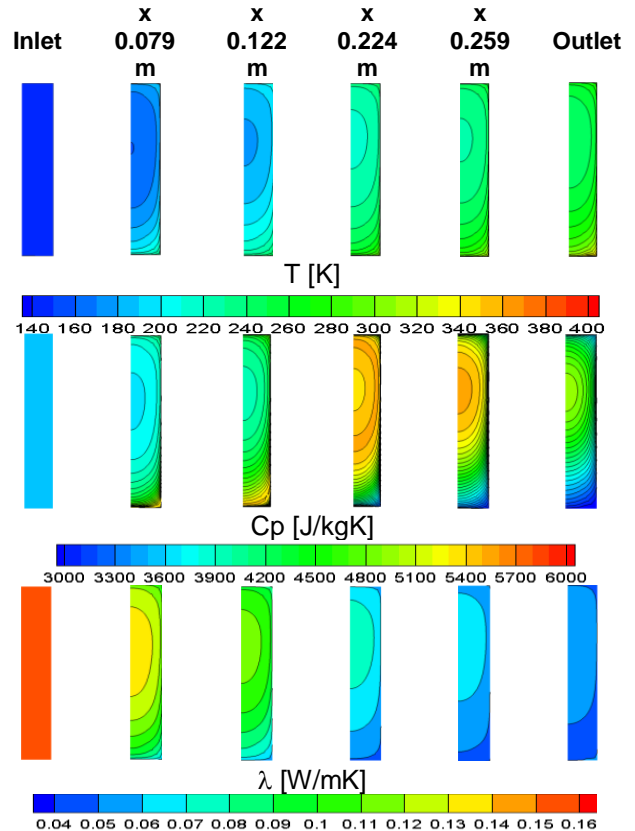


Figure 17 – Fields of fluid temperature, specific heat and thermal conductivity at six slices

Furthermore, from  $x = 0.122$ , the fluid core is characterized by low values of density (thus, high velocity) and high values of specific heat. Here a large part of the fluid exhibits the highest values of specific heat while relative low values of thermal conductivity are detected. This could result in a situation to be difficultly managed, since a deterioration of the fluid thermal performances could be observed [17]; however, in the present tests this phenomenon is not so significant since no local overheating is observed. The reasons may be encountered in the high value of the wall roughness and fluid pressure conditions, sufficiently far from the critical point.

Another significant phenomenon, linked to the contemporary presence of different fluid “phases” inside the channel is the “distortion” of y-direction velocity profile near the bottom part of the channel, as depicted by Figure 18. At the beginning, the typical behaviour of thermally and hydro-dynamically developing flow seems to be observed but from the section  $x = 0.100$  m,

the fluid seems to “accelerate” in the lower part of the channel. In fact, it is hotter near the bottom surface and density is lower. This behaviour tends to be more significant at the exit section because the fluid is composed only by a supercritical vapour.

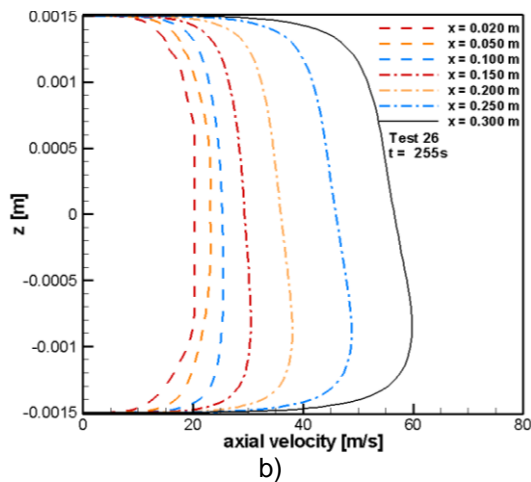


Figure 18 - Axial velocity profiles: test 26.

## 8. CONCLUSIONS

In this paper, results about the preliminary numerical re-building activity, conducted in the framework of ASI/JAXA Co-operation Program, and concerning the experimental campaign, performed by CIRA through the MTP breadboard is described. Simulations were accomplished by means of 3-D models, including also the inlet and outlet interfaces. Cold flow tests were adopted to evaluate the channel roughness and two hot tests were preliminarily re-built. The NIST real gas model has been considered to describe the trans-critical behavior of the methane by means of the most significant thermo-physical properties. Results in terms of bulk fluid temperature, pressure drops and channel surface temperature values are in very good agreement with the experimental data. Results do not show a dramatic deterioration of the fluid thermal performances because of the high values of mass flow and roughness. The critical conditions on average are reached at  $x/L = 0.4$ : from this section, it is possible to observe that a part of the fluid, near the bottom wall, behaves like a “vapour” while in the upper part keeps behaving like a “liquid”; after  $x/L = 0.76$  (pseudo-critical conditions) the fluid completely behaves like a supercritical gas. Results seem to suggest that the fluid does not reach the fully developed regime because is subject to the pseudo-phase change. The re-building activity is going on in order to simulate other test cases and provide useful information in correspondence with other operative conditions.

## 9. ACKNOWLEDGEMENTS

We would like to express our gratitude to our colleagues Michele Ferraiuolo and Manrico Fragiaco for the significant effort spent for the development and support for the MTP design. Furthermore, we would like to thank Scott Meyer, Zucrow Laboratories, Purdue University, for the professionalism and competences proved by him and his team during all the test phases. Finally, a special acknowledgement is addressed to the colleagues of AVIO, Andrea Schoeller, Daniele Liuzzi and Luigi

Arione for their support in managing executive activities of the program.

## 10. NOMENCLATURE

$a$	[m]	Channel height
$b$	[m]	Channel width
$c_p$	[J/kg K]	Specific heat
$D$	[m]	Diameter
$h$	[W/m <sup>2</sup> K]	Convective heat transfer coefficient
$P$	[Pa]	Pressure
$q$	[W/m <sup>2</sup> ]	Heat flux
$T$	K	Temperature
$V$	[m/s]	Velocity
$x, y, z$	[m]	Spatial coordinates
Special characters		
$\rho$	[kg/m <sup>3</sup> ]	Density
$\lambda$	[W/mK]	Thermal conductivity
$\mu$	[Pa s]	Viscosity
Subscripts		
$av$		Average
$cr$		Critical
$f$		Fluid
$h$		Hydraulic
$pc$		Pseudo-critical
$x$		Local

## 11. REFERENCES

- Huzel, D.K., & Huang, D.H. (1992). Modern Engineering for Design of Liquid-Propellant Rocket Engines, Progress in Astronautics and Aeronautics, AIAA.
- Haeseler, D., Bombelli, V., Vuillermoz, P., Lo, R., Marée, T., & Caramelli, F. (2004). Green Propellant Propulsion Concepts for Space Transportation and Technology Development Needs. In Proc. 2<sup>nd</sup> International Conference on Green propellants for Space Propulsion, Cagliari, Italy.
- Accettura, A.G., Mascanzoni, F., Ierardo, N. (2002). Investigations and Considerations about Reusable LOX/HC Engines as Key Technologies for Future Launch Vehicles. In Proc. 38<sup>th</sup> AIAA/ASME/SAE/ASEE Joint Propulsion Conference & Exhibit, 7-10 July, Indianapolis, Indiana, paper AIAA-2002-3846.
- de Lillis, A., Balduccini, M., & D’Aversa, E. (2007). The LOX-Methane Upper Stage Motor Development for the Lyra Launch Vehicle. In Proc. 58<sup>th</sup> International Astronautical Congress (IAC-2007), Hyderabad, India.
- Tomita, T., Ueda, S., Kawashima, H., Onodera, T., Kano, Y., Kubota, I., & Munenaga, T. (2011). Status of Experimental Research on High Performance Methane-Fueled Rocket Thrust Chamber. In Proc. 47<sup>th</sup> AIAA/ASME/SAE/ASEE Joint Propulsion Conference & Exhibit, 31 July - 03 August, San Diego, California, paper AIAA-2011-5935.
- V. Salvatore, et al. (2012). Design and Development of a LOX/LCH4 Technology Demonstrator. In Proc. 48<sup>th</sup> AIAA/ASME/SAE/ASEE Joint Propulsion Conference, 30 July-01 August, Atlanta, USA, paper AIAA-2012-3935.

7. Cornelisse J.W., Schoyer H.F.R., Walker K.F., Rocket Propulsion and Spaceflight, Butterworth-Heinemann, 2007.
8. Sutton G.P., Biblarz O., Rocket Propulsion Elements, John Wiley & Sons, 2010, ISBN-9780470080245.
9. Collins J., Hurlbert E., Romig K., Melcher J., Hobson A., Eaton P., Sea-Level Flight Demonstration & Altitude Characterization of a LO<sub>2</sub>/LCH<sub>4</sub> Based Ascent Propulsion Lander, Proceedings of the 45th AIAA/ASME/SAE/ASEE Joint Propulsion Conference & Exhibit, 3-5 August, 2009, AIAA Paper 2009-4948.
10. Huzel D.K., Huang D.H., Modern Engineering for Design of Liquid-Propellant Rocket Engines, 1992.
11. Panelli M., Cardillo D., Ricci D., Roncioni P., Battista F., The HYPROB Liquid Rocket Engine Demonstrator: CFD Modeling and Simulations, 4th Space Propulsion Conference, 19-22 May, Cologne, 2014.
12. Nathman C.N., Niehaus J., Sturgis J.C., Le A., and Yi J., Preliminary Study of Heat Transfer Correlation Development and Pressure Loss Behavior in Curved High Aspect Ratio Coolant Channels, Proceedings of the 44th AIAA/ASME/SAE/ASEE Joint Propulsion Conference, Hartford, Connecticut, 2008.
13. F. Battista, et al., Experimental Investigation of Methane in Transcritical Conditions, Proceedings of the 50th AIAA/ASME/SAE/ASEE Joint Propulsion Conference, 28-30 July, Cleveland, USA, 2014.
14. NIST Chemistry WebBook, REFPROP v7, <http://webbook.nist.gov/chemistry/fluid/>.
15. Pizzarelli M., Nasuti F. and Onofri M., CFD Analysis of Transcritical Methane in Rocket Engines Cooling Channels, Journal of Supercritical Fluids, Vol. 62, 2012, pp. 79-87.
16. Pizzarelli M., Urbano A., Nasuti F., Numerical Analysis of Deterioration in Heat Transfer to Near-Critical Rocket Propellants, Numerical Heat Transfer, Vol. 57, 2010, pp. 297-314.
17. Negishi H., Daimon Y., Yamanishi N., Ohnishi Y., Numerical Investigation of Supercritical Coolant Flow in Liquid Rocket Engine, Proceedings of the 46th AIAA/ASME/SAE/ASEE Joint Propulsion Conference, Nashville, 2010.
18. Ansys Fluent User's Guide, v14.0., Ansys Inc., Canonsburg, PA.
19. Kreith F., Bohn M.S., Principles of Heat Transfer, 6th Ed., Brooks/Cole, 2000.
20. ECOSIMPRO User's Guide, EA Internacional, Magallanes, Madrid, Spain.
21. Ferraiuolo M., Ricci D., Battista F., Roncioni P., Salvatore V., Thermo-structural and Thermo-fluid Dynamics Analyses supporting the Design of the Cooling System of a Methane Liquid Rocket Engine, Proceedings of the ASME International Mechanical Engineering Congress & Exposition (IMECE2014), November 14-20, Montreal, Canada, 2014, paper IMECE2014-36998.
22. Ricci D., Battista F., Salvatore V. and Fragiaco M., Methane Transcritical Behavior in the Cooling System of the Hyprob-Bread LOX/LCH<sub>4</sub> Demonstrator Rocket Engine, Proceedings of the ASME 2015 International Mechanical Engineering Congress & Exposition (IMECE2015), November 13-19, 2015, Houston, USA